Seismic Hazard Maps for Haiti

Arthur Frankel,[a] M.EERI, Stephen Harmsen,[b] Charles Mueller,[b] Eric Calais,[c] and Jennifer Haase[c] M.EERI

We have produced probabilistic seismic hazard maps of Haiti for peak ground acceleration and response spectral accelerations that include the hazard from the major crustal faults, subduction zones, and background earthquakes. The hazard from the Enriquillo-Plantain Garden, Septentrional, and Matheux-Neiba fault zones was estimated using fault slip rates determined from GPS measurements. The hazard from the subduction zones along the northern and southeastern coasts of Hispaniola was calculated from slip rates derived from GPS data and the overall plate motion. Hazard maps were made for a firm-rock site condition and for a grid of shallow shear-wave velocities estimated from topographic slope. The maps show substantial hazard throughout Haiti, with the highest hazard in Haiti along the Enriquillo-Plantain Garden and Septentrional fault zones. The Matheux-Neiba Fault exhibits high hazard in the maps for 2% probability of exceedance in 50 years, although its slip rate is poorly constrained. [DOI: 10.1193/1.3631016]

INTRODUCTION

Seismic hazard maps for Haiti are a prerequisite for establishing scientifically defensible building codes for use in the rebuilding process from the 12 January 2010 M7.0 earthquake. These maps also provide important information for emergency response and preparedness, planning by businesses and other organizations, government decision-making, and hazard awareness for individuals, among many other uses. Probabilistic seismic hazard maps are essential tools that help to mitigate the loss of life and property from future earthquakes. For example, design values in the seismic provisions of the International Building Code (IBC) used for new buildings in the United States are based on the U.S. national seismic hazard maps (Frankel et al. 2000, Petersen et al. 2008).

This paper describes a set of new probabilistic seismic hazard maps we have made for Haiti. These maps are an initial step toward quantifying the seismic hazard and will be improved as more data become available on fault slip rates, chronology of prehistoric large earthquakes on the major faults and subduction zones, crustal deformation, ground-motion excitation and attenuation, and site response. It is also essential to develop a comprehensive catalog of active faults for the region. More details about these hazard maps are given in Frankel et al. (2010).

While the hazard maps shown in this article contain the entire island of Hispaniola and the easternmost portion of Cuba, we stress that these maps are incomplete for the

[a] U.S. Geological Survey, University of Washington, Box 351310, Seattle, WA 98195
[b] U.S. Geological Survey, MS 966, Box 25046, Denver, CO 80225
[c] Purdue University, Dept. of Earth and Atmospheric Sciences, West Lafayette, IN 47907

Earthquake Spectra, Volume 27, No. S1, pages S23–S41, October 2011; © 2011, Earthquake Engineering Research Institute

Dominican Republic and eastern Cuba. These maps do not include some of the sources of large earthquakes that would affect eastern Hispaniola, such as the Mona Passage between Hispaniola and Puerto Rico and the plate boundary along the Puerto Rico trench to the northeast of Hispaniola.

TECTONIC SETTING, FAULTS, AND EARTHQUAKE HISTORY

The boundary between the Caribbean and North American Plates in the area of Hispaniola is a wide and complex zone that accommodates the 20 mm/yr of east northeast motion of the Caribbean Plate relative to the North American Plate (DeMets et al. 2000). This oblique motion is partitioned between subduction zones on the northern and southern coasts, two major strike-slip faults cutting through the northern and southern parts of the island, and poorly known thrust faults within the island (Mann et al. 1984, 1995; Calais et al. 2002). The complexity of the plate boundary is thought to be largely due to the impingement of Hispaniola on the Bahama Platform, which is an area of thickened crust on the North American Plate north of Hispaniola (Mann et al. 2002).

A map of the major tectonic features included in the hazard calculation is depicted in Figure 1. Three crustal faults were considered explicitly in the hazard maps: the Enriquillo-Plantain Garden and Septentrional strike-slip faults and the Matheux-Neiba thrust fault. The Enriquillo-Plantain Garden and Septentrional Faults have been recognized as major tectonic features for decades and the earthquake potential of these faults had been widely reported (e.g., Mann et al. 1995, Calais et al. 2002, Manaker et al. 2008). The Enriquillo-Plantain Garden fault zone continues to the west and extends to Jamaica. No geologically-measured slip rate has been determined for the Enriquillo-Plantain Garden fault zone. Prentice et al. (2003) trenched several locations along the Septentrional Fault in the Dominican Republic. They estimated a slip rate of 6–12 mm/year for the fault from geologic offsets. Based on evidence from the trenches, they estimated a recurrence time of 800–1200 years for large earthquakes rupturing this location. The Septentrional Fault continues to the west as the Oriente fault zone that passes south of Cuba. The Matheux-Neiba Fault is a poorly studied thrust fault just to the north of Port-au-Prince that may currently accommodate north–south convergence (Mann et al. 1984, Pubellier et al. 2000).

It is critical to note that there are other fault zones in Haiti and the Dominican Republic that are not explicitly included in this hazard assessment, because of the lack of slip rate measurements or trenching that could provide information on their recurrence times. Use of the spatially smoothed seismicity in the hazard calculation (see section on Methodology of Hazard Calculation) is meant to account for some of the hazard from unmodeled faults. However, it is imperative that a systematic investigation of the active faults in Hispaniola be done to quantify their slip rates and/or recurrence rates.

The 12 January 2010 earthquake is thought to have occurred on a steeply dipping fault located just north of the main trace of the Enriquillo-Plantain Garden Fault, based on fault modeling by Calais et al. (2010) of coseismic deformation measured with GPS instruments and interferometric synthetic aperture radar (InSAR). This fault, which dips steeply to the north, has been named the Léogâne Fault. Hayes et al. (2010) found a similar result from modeling InSAR data, coral uplifts, and teleseismic waveforms, but also propose a minor component of coseismic slip on two other faults, one of which may be the main trace of the Enriquillo-Plantain Garden Fault. The treatment of the Léogâne Fault in probabilistic

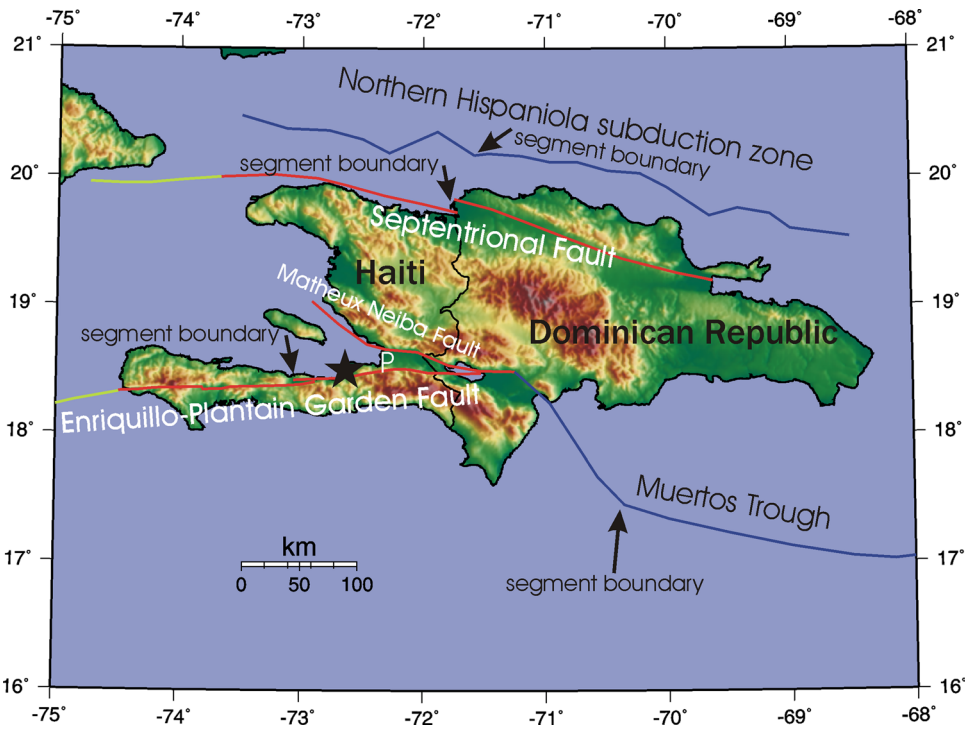

Figure 1. Map of crustal faults (red and green) and subduction zones (blue) used in the hazard calculations. Green portion of faults were treated separately (see text). Inferred segment boundaries are shown by arrows. "P" denotes the location of Port-au-Prince. The star is the epicenter of the M7.0 12 January 2010 earthquake.

seismic hazard assessment is problematic, since there are no estimates of slip rate for this particular fault, or estimates of its recurrence time. Some of the slip rate we have assigned to the Enriquillo-Plantain Garden Fault may be taken up by adjacent faults such as the Léogâne Fault. The seismic hazard we determine for the Enriquillo-Plantain Garden Fault includes high probabilistic ground motions for locations adjacent to the fault, including the area above the Léogâne Fault. Also, the spatially smoothed seismicity component of the hazard calculation also contributes to the hazard estimate for this area.

Haiti has an extensive history of major earthquakes prior to the January 2010 earthquake (Scherer 1912, Kelleher et al. 1973, McCann 2006, see compilation in Ali et al. 2008). An earthquake in 1701 destroyed the city of Léogâne, west of Port-au-Prince (Scherer 1912). A large earthquake in November 1751 caused severe damage to Port-au-Prince and is thought to have been located on the Enriquillo-Plantain Garden Fault. McCann (2006) estimated a magnitude of 7.5 for this earthquake, based on intensity reports. The magnitudes of the historic earthquakes quoted here are moment magnitudes. Prentice et al. (2010) found offsets along the Enriquillo-Plantain Garden Fault trace that may be associated with the November 1751 earthquake. In June 1770 a large earthquake occurred to the west of Port-au-Prince with an estimated magnitude of 7.5 (McCann 2006), perhaps on the portion of the

Enriquillo-Plantain Garden Fault in southwestern Haiti. A moderate or large earthquake occurred to the west of Port-au-Prince in 1860 (Kelleher et al. 1973), again possibly on the Enriquillo-Plantain Garden fault zone. Two large earthquakes in 1842 and 1887 occurred in northern Hispaniola, possibly associated with the Septentrional Fault. McCann (2006) estimated magnitudes of 8.0 and 7.75, respectively, for these earthquakes.

Subduction zones are situated off the northern and southern coasts of Hispaniola (Figure 1). The northeastern coast is located on an especially active subduction zone. A sequence of four large ($M \geq 7.0$) thrust earthquakes occurred along this zone from 1946 to 1953. The largest of these events on 4 August 1946 had a surface wave magnitude of about 8.0 (Dolan and Wald 1998). The aftershocks of this event indicate that it ruptured a 200 km-long portion of the subduction zone (Dolan and Wald 1998).

The Muertos Trough off the southeast coast of Hispaniola has some of the characteristics of a subduction zone, such as northward dipping oceanic crust and seismicity, and an accretionary prism (Ladd et al. 1977, Byrne et al. 1985, McCann 2006), although ten Brink et al. (2009) contend that it is a thrust zone without subduction of oceanic crust. A tsunamigenic earthquake in October 1751, only one month before the November 1751 earthquake to the west, may have ruptured a portion of this subduction zone (McCann 2006). A M_s 6.7 thrust earthquake occurred at 32 km depth beneath the northern slope of the Muertos Trough in 1984 (Byrne et al. 1985). The east end of the Enriquillo-Plantain Garden fault zone transitions into the west end of the Muertos Trough, although the details are not clear and these faults may not be connected.

Figure 2 shows a map of the seismicity from 1900 to 2009 for Hispaniola. Earthquakes with magnitudes greater than 4.0 are shown, although the catalog is not complete down to this magnitude until after 1963 (see section on spatially smoothed seismicity). This catalog was derived from: 1) the U.S. Geological Survey (USGS) Preliminary Determination of Epicenters (PDE) catalog from 1973 to February 2010, 2) the Engdahl and Villasenor (2002) catalog from 1902 to 2000, and 3) the International Seismic Centre (ISC) catalog from 1911 to January 2008. The catalog has been declustered to remove aftershocks, foreshocks, and other dependent events using the procedure of Mueller et al. (1997). The seismicity map shows more earthquakes with $M \geq 4.0$ in the eastern portion of Hispaniola, with the largest concentration of shallow earthquakes located along the northeastern subduction zone. There is a notable nest of deep (>100 km) earthquakes under eastern Hispaniola. There have been a substantial number of shallow $M \geq 4$ earthquakes in Haiti since 1963.

A map of seismic hazard for the Caribbean, including Haiti, was produced by Tanner and Shepherd (1997) as part of the Global Seismic Hazard Assessment Program (see Shedlock 1999). This hazard map was based on the instrumental seismicity of the region ($M \geq 4.0$) from 1963 to 1993. They used a probabilistic method based on extrapolating the return times from the ground motions calculated for the earthquakes in this catalog, using a Gutenberg-Richter recurrence relation. They did not include specific faults or subduction zones, so that these maps did not fully capture the higher seismic hazard expected near these earthquake sources.

Mueller et al. (2010) published seismic hazard maps for Puerto Rico. Their maps included hazard from the northeastern subduction zone and the Septentrional Fault, as well as the earthquake sources east of Hispaniola, including the Mona Passage.

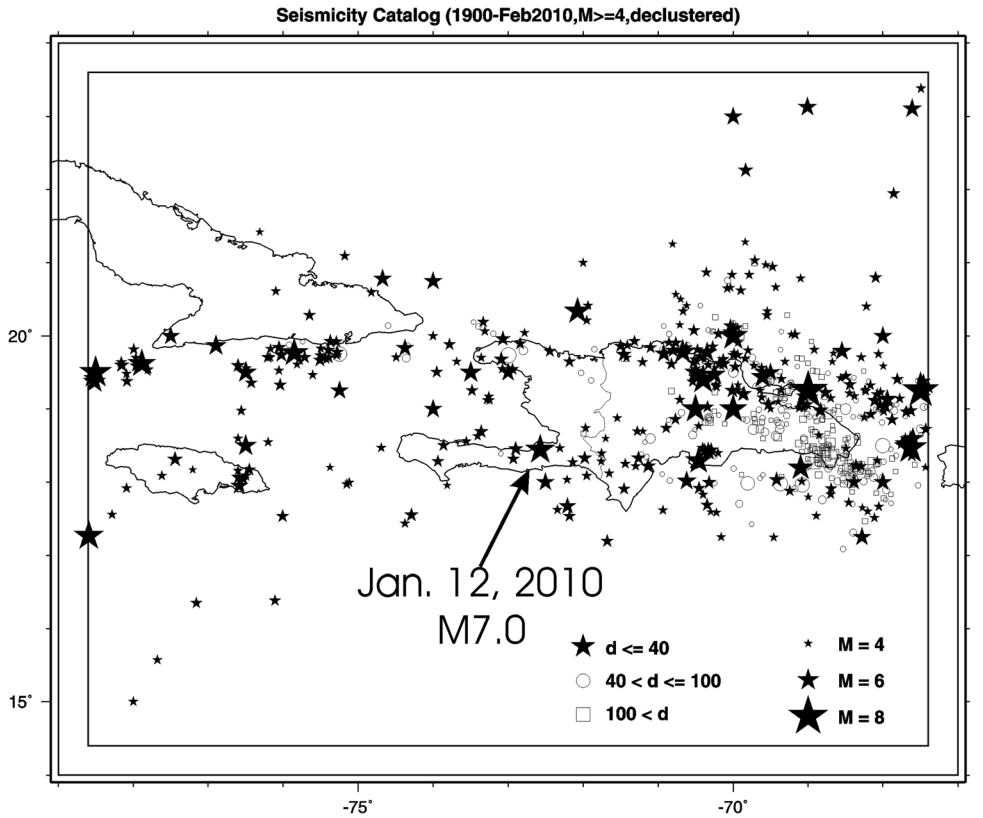

Figure 2. Map of epicenters of earthquakes since 1900 with magnitudes of 4 or larger. Symbol type is keyed to hypocentral depth in km. Symbol size is scaled with magnitude. Dependent events (e.g., aftershocks, foreshocks) have been removed.

METHODOLOGY OF HAZARD CALCULATION

We followed the basic methodology used to make the U.S. national seismic hazard maps since 1996 (Frankel et al. 1996) and the recent hazard maps for Puerto Rico by Mueller et al. (2010). Probabilistic seismic hazard assessment involves calculating seismic hazard curves that describe the annual frequencies of exceeding specified ground-motion values (Cornell 1968). These hazard curves are determined by summing the annual frequencies of exceedance at any given ground-motion value for all the earthquake sources considered. For each source (e.g., a fault or a grid cell with a seismicity rate), the frequency of exceedance of a specified ground-motion value at the site of interest is calculated from the product of the rate of earthquakes for that source and the probability that an earthquake at that source location will produce ground motions larger than the specified value at the site. Seismic hazard maps typically depict ground-motion values that have a particular annual frequency of being exceeded, which can also be expressed as a probability of being exceeded over a given time period. In this paper, we assume a Poissonian or time-independent model

of earthquake recurrence such that the time of the previous large earthquake on a fault is not considered in the calculation. We are not considering the hazard from aftershocks.

We combined the hazard from specific faults and subduction zones with that derived from the spatially smoothed seismicity. Here the term "hazard" refers to the frequency of exceedance as a function of ground-motion value. We used the spatially smoothed seismicity to quantify the hazard from shallow earthquakes not on the major faults, as well as that from deep Benioff-zone earthquakes. This method is described in detail in Frankel (1995). In order to estimate earthquake recurrence rates from fault slip rates, recurrence models must be specified that describe the frequency-magnitude distribution of earthquakes on a fault. Two alternative recurrence relations were applied to form a probability distribution to calculate the hazard from crustal faults and subduction zones. The first recurrence relation is called the characteristic model, where the seismic moment is taken up in earthquakes that rupture the entire fault or fault segments. A characteristic moment magnitude is determined from either a fault segment length or the entire length of a mapped fault trace. The second relation is the truncated Gutenberg-Richter (GR) relation where the number N of earthquakes equal to or larger than moment magnitude M is given as $log\ N = a - bM$, where a is the log of the seismic activity and b is the slope. In this study, we used a b-value of 1.0 for the GR relation on the three crustal faults considered. We found that the ground motion values in the hazard maps were not significantly different between using $b = 0.75$ and $b = 1.0$ for the Enriquillo-Plantain Garden Fault. The GR relation was truncated at minimum magnitudes of 6.5 or 7.0, so as not to overpredict the rate of earthquakes between magnitudes 5 and 7. Note that the hazard from earthquakes between M5.0 and 7.0 is calculated from the spatially smoothed seismicity. The GR relation is also truncated at high magnitudes at the characteristic magnitude. We also include random (aleatory) uncertainty in the determination of the characteristic magnitude.

Frankel et al. (1996) describes in detail how earthquake rates are calculated from slip rates using these two models and provides the relevant formulas. A seismic moment rate for each fault or fault segment is calculated from the slip rate, segment length, seismogenic depth (assumed here to be 15 km), and shear modulus. In the characteristic model this seismic moment rate is taken up by earthquakes with magnitudes around the characteristic magnitude for that segment. For the GR model, this seismic moment is produced by the sum of seismic moments from earthquakes between the minimum magnitude and the characteristic magnitude, with an exponential distribution. It is important to stress that we do not determine recurrence times on these faults from the catalog of recent earthquakes around these faults. We use the slip rates to determine recurrence times on the faults. We do use the rate of moderate and large historic earthquakes as a check on the recurrence rates derived from the slip rate and recurrence models.

CRUSTAL FAULTS

The seismic hazard from the crustal faults is determined from slip rates derived from GPS measurements, with the rates of historic large earthquakes as constraints. Table 1 lists the slip rates, characteristic (maximum magnitudes), and predicted rates of moderate and large earthquakes for each fault and subduction zone considered here. Calais et al. (2002) and Manaker et al. (2008) derived a slip rate of 7 mm/yr for the Enriquillo-Plantain Garden

Table 1. Parameters used in hazard calculation for faults and subduction zones

Crustal fault or subduction zone	Slip rate (mm/yr)	Mchar	Mmin	Predicted Annual Rate $M \geq 6.5$	Predicted Annual Rate $M \geq 7.0$
Enriquillo-Plantain Garden	7	7.7	6.5	0.016	0.0053
Septentrional	12	7.8	6.5	0.021	0.0078
Matheux- Neiba	1	7.7	6.5	0.0034	0.0012
Eastern portion of northern subduction zone	11	8.0	8.0	0.005	0.005
Western portion of northern subduction zone	2.5	8.0	7.5	0.00088	0.00088
Muertos Trough subduction zone, Neiba segment (west portion)	7	8.0	7.5	0.0030	0.0030
Muertos Trough subduction zone central segment	7	8.0	7.5	0.0050	0.0050

Fault zone based on fitting GPS measurements with a block model. The fault trace shows a possible segment boundary at 73° W longitude. Here the fault makes a left, transtensional step forming the Miragoane pull-apart basin (Momplaisir 1986). This is also the approximate westward limit of the rupture zone of the January 2010 earthquake as determined from modeling teleseismic waveforms (Hayes et al. 2010) and from the aftershock distribution. The characteristic earthquake magnitude for the Enriquillo-Plantain Garden Fault was estimated from the distance between the eastern end of the Enriquillo-Plantain Garden Fault and this inferred segment boundary. The length of this segment yields a moment magnitude of 7.7, based on the relations of Wells and Coppersmith (1994) derived for all fault types. We use this as the characteristic magnitude in the characteristic portion of the distribution and as the maximum magnitude for the GR portion of the distribution. The maximum magnitude of 7.7 for this fault is reasonable, given the estimated magnitude of 7.5 for the November 1751 and 1770 earthquakes inferred to have occurred on this fault (McCann 2006).

The western, offshore portion of the Enriquillo-Plantain Garden Fault (green portion of trace in Figure 1) was treated separately from the rest of the fault, since little is known of its earthquake history. Based on the length of this segment, we estimated a characteristic magnitude of 7.6. We assume vertical dip for the Enriquillo-Plantain Garden Fault. There is some evidence that the fault dips steeply to the south from geologic mapping (Prentice et al. 2010). Nonvertical fault dip can affect the determination of the fault area and substantially alter estimates of recurrence time, if the characteristic magnitude is determined only from fault length rather than fault area. Since it is not clear whether the southward dip of this fault is representative of its average behavior, we decided to use the vertical dip for these initial hazard maps.

We developed a magnitude-frequency relation for the Enriquillo-Plantain Garden Fault by choosing 0.5 weight for the characteristic model and 0.5 weight for the truncated GR model. In other words, we assume that 50% of the seismic moment is released as characteristic earthquakes and 50% is released in earthquakes that follow the GR distribution. A minimum magnitude of 6.5 was used for the GR model, following the procedure of the U.S. national maps (Frankel et al. 1996). It is possible that some of the M6.5–7.0 earthquakes in

the GR model may occur on shorter faults adjacent to the main trace of the Enriquillo-Plantain Garden Fault, such as the Léogâne Fault. In this analysis we place all of the earthquakes calculated from the slip rate on the main trace of the fault.

The predicted rates of moderate and large earthquakes from our model of the Enriquillo-Plantain Garden Fault are comparable to the observed ones. Our model predicts a mean annual rate of $M \geq 6.5$ earthquakes of 0.016 for the onshore portion of the Enriquillo-Plantain Garden Fault (red trace in Figure 1). If we assume the 1751, 1770, and 1860 earthquakes were greater or equal to M6.5, and include the January 2010 earthquake (M7.0), the average observed recurrence rate for $M \geq 6.5$ is $0.014\ {}^{+0.011}_{-0.007}$, similar to our predicted rate. Here the observed rate is the maximum likelihood rate since 1720 and the error bounds are one standard deviation (based on Weichert 1980). The predicted rate for $M \geq 7.0$ is 0.0053, about 53% of the observed rate of $0.010\ {}^{+0.010}_{-0.005}$ (using the 1751, 1770, and 2010 earthquakes). However, the predicted rate is within one standard deviation of the observed rate, given the small number of earthquakes.

Based on the recent analysis of GPS data by Calais et al. (2010), we assigned a slip rate of 12 mm/yr for the Septentrional fault zone. This is at the upper end of the 6–12 mm/yr estimated by Prentice et al (2003) from geologic offsets on the eastern portion of the fault. The 12 mm/yr for the Septentrional Fault and the 7 mm/yr for the Enriquillo-Plantain Garden Fault add up to about 19 mm/yr of left-lateral motion, similar to that required from the overall plate motion determined by DeMets et al. (2000).

The characteristic (maximum) magnitude of the Septentrional Fault was estimated by assuming that the offset at 71.7° W longitude represented a segment boundary. The length of the eastern segment implies a maximum magnitude of 7.8. Again, this is consistent with the estimated magnitudes of 8.0 and 7.75 for the 1842 and 1887 earthquakes, respectively (McCann 2006). Mann et al. (1998) proposed that the active trace of the Septentrional Fault in northwest Dominican Republic is actually buried beneath alluvial deposits and lines up with the trace of the fault just offshore of the northern coast of Haiti. This possibility should be evaluated for future hazard maps. We found that giving equal weight for the characteristic and GR models for the Septentrional Fault produced a rate of $M \geq 6.5$ earthquakes substantially higher than that observed for this fault. Therefore, we chose a weight of 0.33 for the GR model and 0.67 for the characteristic model. This implies that 67% of the seismic moment is released in characteristic earthquakes and 33% in earthquakes that follow the GR distribution. The model predicts a 0.021 rate of $M \geq 6.5$ earthquakes on the portion of the fault shown in red in Figure 1. The catalog contains a few earthquakes of this size that may have occurred on the fault. The earthquakes in 1842 and 1887 imply a maximum likelihood rate of $0.0065\ {}^{+0.0085}_{-0.0042}$ (assuming catalog start at 1700) for $M \geq 7.0$. This is comparable to the predicted rate of 0.0078 for $M \geq 7.0$ for this fault. Based on two events found in trenching in the eastern portion of the fault, Prentice et al. (2003) estimated a 1,000-year recurrence time at this location. However, earthquakes with magnitudes around 7.0 may not always produce surface displacements measurable in a trench. We treated the western portion of the Septentrional Fault separately (green portion of trace in Figure 1), because of the large uncertainty in its earthquake history. We estimated a characteristic magnitude of 7.5 for this portion of the fault from its length.

The third crustal fault specified in the hazard analysis is the Matheux-Neiba Fault, a poorly studied thrust fault to the north of Port-au-Prince. We chose to use a slip rate of

1 mm/yr for this fault. This is the approximate upper limit of the slip rate of this fault that is allowable from fitting the GPS data (Calais et al. 2010). The length of this fault yields a maximum magnitude of 7.7. We used a distribution with 50% weight for the characteristic model and 50% weight for the GR model. The predicted annual rates for $M \geq 6.5$ and $M \geq 7.0$ earthquakes are 0.0034 and 0.0012, respectively, much lower than the recurrence rates predicted for the Enriquillo-Plantain Garden and Septentrional Faults.

SUBDUCTION ZONES

We divided the subduction zone off of the northern coast into two segments (Figure 1) at about 71.5° W longitude because there is a gradual change in strike of the subduction zone boundary starting at about this location. Modeling the GPS data also indicates that the slip rate is higher for the eastern portion of the zone than the western portion (Manaker et al. 2008). The rate of $M \geq 4.0$ earthquakes is also higher in the eastern portion than the western one (Figure 2).

We used a convergence rate of 11 mm/yr to estimate the rates of great earthquakes on the eastern portion of the northern subduction zone. This is the total rate of motion perpendicular to the plate boundary determined by DeMets et al. (2000) from an analysis of GPS data. Of course, a portion of this convergence is probably accommodated along the Muertos Trough and by faults throughout Hispaniola. GPS data suggest that the rate of convergence along the northeastern subduction zone may be lower (Manaker et al. 2008). We used a characteristic earthquake model with a moment magnitude of 8.0, consistent with the range of surface wave magnitudes determined for the 1946 earthquake that ruptured this zone (Dolan and Wald 1998). Using the 11 mm/yr slip rate yields a recurrence rate of 0.005. This is the same rate and characteristic magnitude applied in the Mueller et al. (2010) hazard maps for Puerto Rico.

The hazard from the western portion of the northern subduction zone was estimated from the slip rate of 2.5 mm/yr derived from GPS measurements by Manaker et al. (2008). A maximum magnitude of 8.0 was assumed, based on the magnitude of the 1946 earthquake on the eastern portion of the subduction zone. We gave half weight to a characteristic model and half weight to a GR model. We decided to increase the minimum magnitude to 7.5 for this portion of the subduction zone and for the Muertos Trough. This was necessary to reduce the predicted rates of $M \geq 7.0$ earthquakes, to bring them more in accordance with the historic rate.

The Muertos Trough was divided into two segments based on the change of strike causing more oblique subduction east of about 70° W longitude (Figure 1). The slip rate used for the Muertos Trough was 7 mm/yr, based largely on the results of GPS modeling. This is consistent with the idea that the 7 mm/yr slip on the Enriquillo-Plantain Garden Fault continues to the east and is accommodated in the Muertos Trough. We used an Mmax of 8.0, Mmin of 7.5, and equally weighted characteristic and GR models in the hazard calculation. The model predicts relatively high rates for $M \geq 7.5$ earthquakes of 0.003 for the western segment and 0.005 for the eastern segment. The 1751 earthquake is the only large earthquake in the 300-year historic record that may be associated with this zone (McCann 2006). Slip may be very oblique to the strike of the trough along its eastern portion. This may

cause lower coupling along the eastern part of the Muertos Trough, so that our predicted earthquake rate, which assumes full coupling, may overestimate the hazard there.

SPATIALLY SMOOTHED SEISMICITY

The final part of the hazard calculation used the spatially smoothed seismicity to incorporate the hazard from random earthquakes not on the major crustal faults. We first estimated completeness times of the catalog for various threshold magnitudes by examining plots of cumulative number of events as a function of time. We concluded that the catalog for $M \geq 4.0$ was approximately complete since 1963 and the $M \geq 6.0$ earthquakes were complete from 1915. We divided the seismicity into three depth ranges of 0–40 km, 41–100 km, and 101 km and deeper, and applied the spatial smoothing to each depth range separately. We found a maximum likelihood *b*-value of 0.74 ± 0.07 for the declustered catalog of earthquakes since 1963 with depths less than 40 km. Earthquakes with a depth of between 41 km and 100 km also had the same *b*-value. Therefore, we used a *b*-value of 0.75 in the hazard calculation for all the depth ranges, rounding to the nearest 0.05. Maximum-likelihood *a*-values were calculated on a grid with spacing of 0.1 degrees in latitude and longitude. A Gaussian smoothing function with a correlation distance of 50 km was used for each depth range, the same correlation function applied in the U.S. national seismic hazard maps for $M \geq 4$ earthquakes in the western United States. The hazard was calculated separately for each depth range using the attenuation relations appropriate for that depth range. The depth of the top of rupture in the hazard calculation was taken to be 10 km for the earthquakes above 40 km, recognizing that the number of earthquakes in most locations decreases with depth. Depths of the top of rupture in the hazard calculation were chosen at 60 km for the 40–100 km depth range and 120 km for the earthquakes greater than 100 km.

We integrated the hazard from M5.0 to M7.0 from the spatially smoothed seismicity. Finite faults with random strikes centered in each seismicity-rate cell were used in the hazard calculations for earthquakes greater than magnitude 6.0, as in Frankel et al. (1996). Point sources were applied to calculate the hazard for magnitudes 5.0 to 6.0.

ATTENUATION RELATIONS

Different sets of attenuation relations were applied depending on the type of earthquake source. We used the same sets of attenuation relations as in the 2008 U.S. national seismic hazard maps (Petersen et al. 2008). For crustal earthquakes, we applied three of the Next Generation of Attenuation (NGA) relations (Boore and Atkinson 2008, Campbell and Bozorgnia 2008, and Chiou and Youngs 2008) with equal weights. These attenuation relations were based on fitting the peak ground accelerations (PGA) and spectral accelerations from a global compilation of strong-motion records from tectonically active areas. These relations contain explicit terms with the shear wave velocity averaged over the top 30 m (V_{S30}) for a site. We decided not to use attenuation relations based on simulated seismograms. We preferred to use attenuation relations based directly on observations from a global collection of large earthquakes. It is especially important to accurately estimate the hazard close to the crustal faults where differences in crustal propagation are not as critical.

For earthquakes on the interface of the subduction zones we used three attenuation relations determined from data from earthquakes in these zones: Youngs et al. (1997), Atkinson and Boore (2003), and Zhao et al. (2006). Weights of 0.25, 0.25, and 0.5 were assigned,

respectively, following the 2008 U.S. national maps. The higher weight for the Zhao et al. (2006) relations was chosen because of the larger amount of data used. They exhibit higher ground motions at close-in distances (<100 km) than either of the other two relations. So we applied a higher weight for Zhao et al. (2006) to capture the epistemic uncertainty in the close-in ground motions from large subduction zone earthquakes. The hazard from deep earthquakes (>40 km) was determined using the equations in Youngs et al. (1997) and Atkinson and Boore (2003), with equal weights, as specified for deep intraslab earthquakes.

Two sets of hazard maps were constructed. One set used a uniform site condition of firm rock with a V_{S30} of 760 m/s. This is the same site condition as applied for the U.S. national maps. The second set of maps included an approximation of the site condition (V_{S30}) in 1 km by 1 km grid cells, based on the topographic slope using the method of Wald and Allen (2007). To calculate ground motions for each cell we used the V_{S30} terms specified by the authors of the NGA relations. For the other attenuation relations, we used the site amplification formula from the Boore and Atkinson (2008) NGA relations. This site amplification formula is a function of V_{S30}, period, and the calculated PGA for a rock site.

HAZARD MAPS FOR FIRM ROCK SITES

Figures 3 and 4 show the PGAs with 10% and 2% probabilities of exceedance (PE), respectively, in 50 years for a firm-rock site condition. All of the hazard maps in this paper

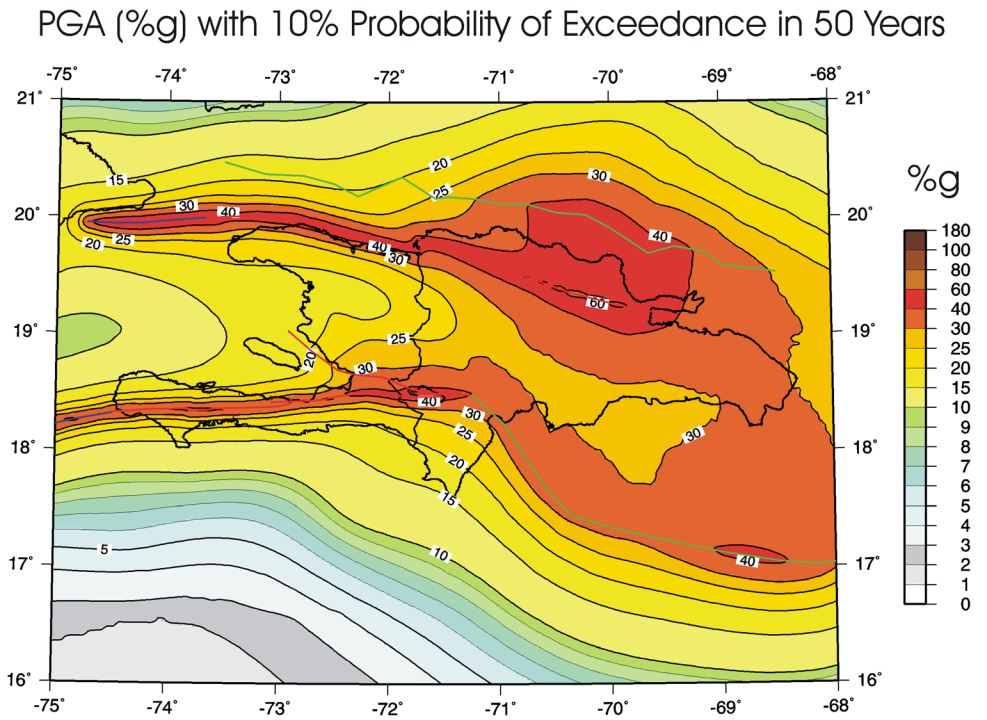

Figure 3. Hazard map of PGA (%g) with 10% probability of exceedance in 50 years, for a firm-rock site condition.

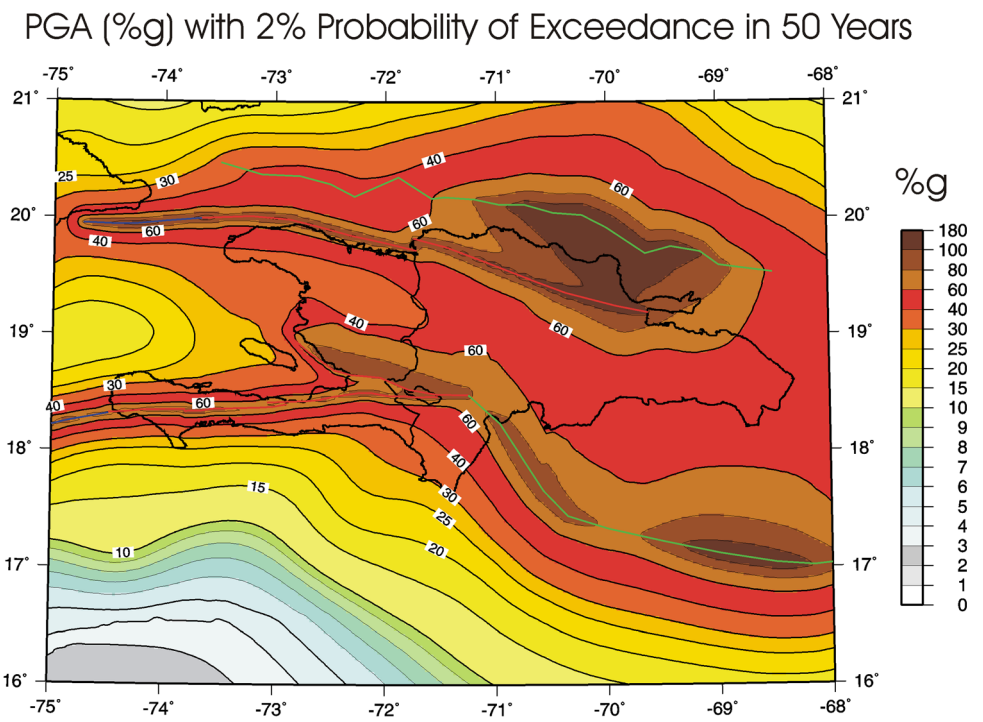

Figure 4. Hazard map of PGA (%g) with 2% probability of exceedance in 50 years, for a firm-rock site condition.

are based on mean hazard curves. The maps show that substantial seismic hazard exists throughout Haiti. There is very high hazard along the Enriquillo-Plantain Garden and Septentrional Faults in Haiti and along the northeastern subduction zone and Muertos Trough. For the 2% PE in 50 years map, high hazard is also apparent along the Matheux-Neiba Fault. The high hazard for this fault at low probabilities is caused by the long recurrence time for this fault determined from the relatively low slip rate of 1 mm/yr. Again, we note that this slip rate is poorly constrained by the GPS data, so the hazard estimate for this fault has large uncertainty.

Mean hazard curves of the different earthquake sources for PGA at a firm-rock site at Port-au-Prince are depicted in Figure 5. At a PE of 10% in 50 years, the hazard is dominated by earthquakes on the Enriquillo-Plantain Garden fault zone. Earthquakes on the Matheux-Neiba fault zone are the next most important contributor at this PE. For a PE of 2% in 50 years, earthquakes on the Enriquillo-Plantain Garden and Matheux-Neiba Faults have about equal contribution to the total hazard calculated for Port-au-Prince. At high annual probability levels greater than 0.025, the spatially smoothed gridded seismicity is the major contributor to the hazard to Port-au-Prince, with the Enriquillo-Plantain Garden Fault the second most important component. However, some of this gridded seismicity may be associated with earthquakes in the Enriquillo-Plantain Garden fault zone.

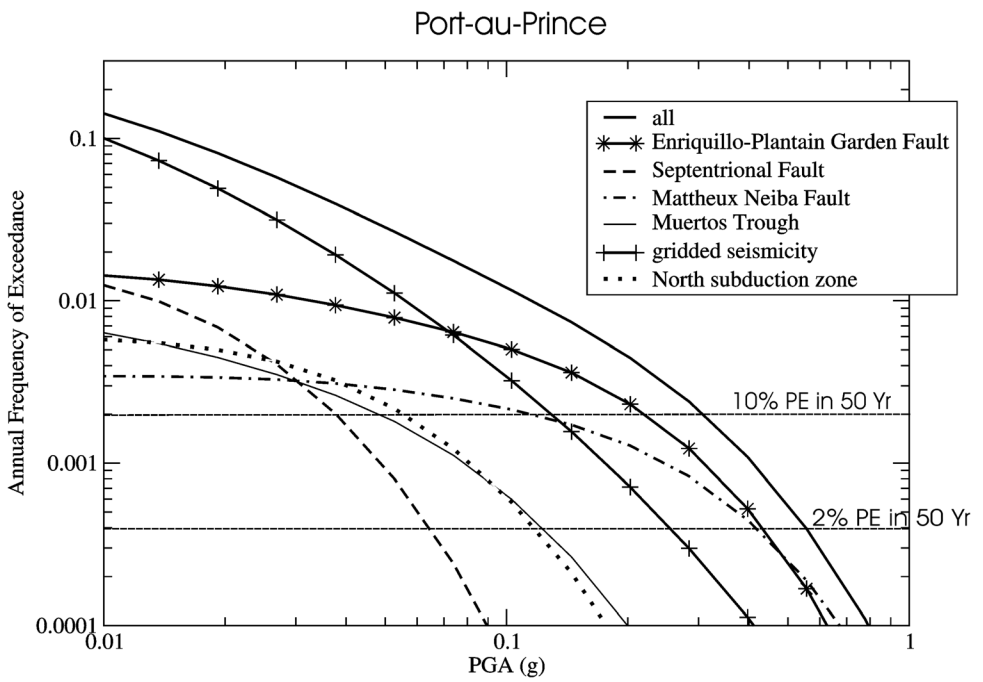

Figure 5. Hazard curves for PGA for Port-au-Prince for the various faults, subduction zones, and gridded seismicity. Horizontal lines represent probabilities of exceedance of 10% and 2% in 50 years.

Figure 6 depicts the hazard maps for 0.5, 1.0, 2.0, and 5.0 Hz spectra accelerations (5% of critical damping) for a PE of 2% in 50 years. The overall appearance of each map is similar to the PGA map at the same PE (Figure 4), with the highest hazard in Haiti occurring along the Enriquillo-Plantain Garden and Septentrional Faults and substantial hazard found throughout the country.

HAZARD MAPS WITH SOIL AMPLIFICATION

The topographic slope was used to estimate the V_{S30} on a 1 km by 1 km grid across Hispaniola (Figure 7, map provided by David Wald, written comm.). This map was based on the methodology of Wald and Allen (2007), who developed an empirical relation between V_{S30} and topographic slope. Areas of low estimated V_{S30} (<360 m/s, stiff or soft soils) in Haiti include portions of the Enriquillo Valley where Port-au-Prince is located and the delta of the Artibonite River at about 19.2° N latitude.

Figure 8 contains the PGA hazard maps with site amplification for PEs of 10% and 2% in 50 years. Because of nonlinear site soil response for high PGAs, the site amplification is more prominent in the 10% PE in 50 years map, which has lower PGAs than the 2% PE in 50 year map. The PGA values in the 10% PE in 50 years map for the soil areas are about 30%–40% larger than those for a firm-rock site condition (Figure 3). Areas on stiffer

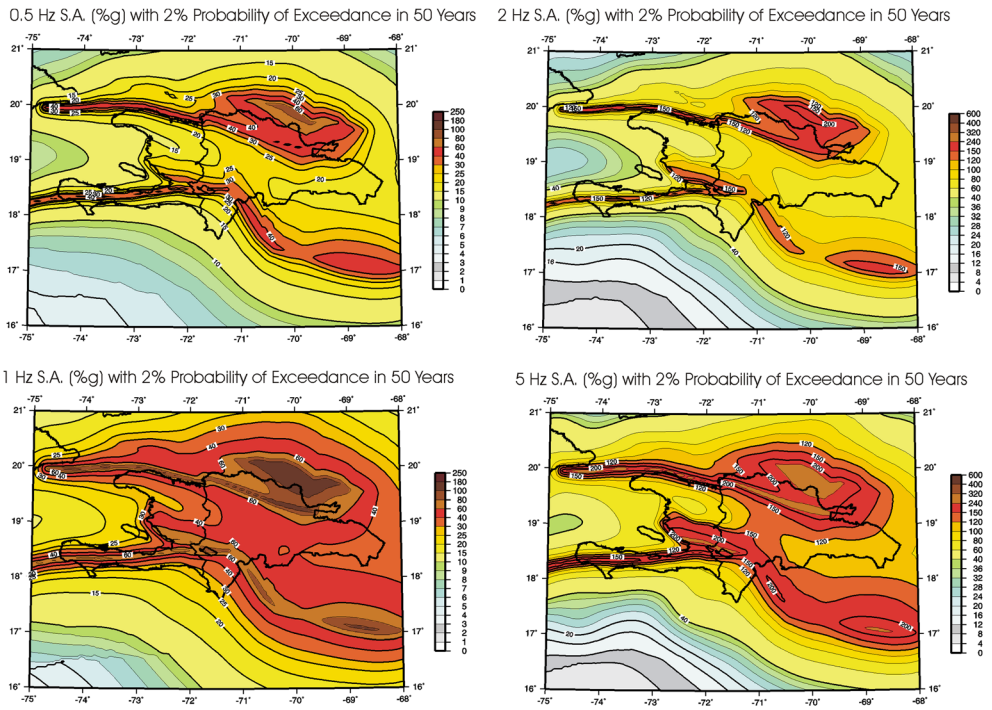

Figure 6. Hazard maps for spectral accelerations (5% of critical damping; %g) for frequencies of 0.5, 1.0, 2.0, and 5.0 Hz, for firm-rock sites. Note that the color scales differ between some of the plots.

materials (V_{S30} around 500 m/s) show amplifications of about 20%. For the maps depicting PGA with 2% PE in 50 years, values are similar along the high hazard areas for the map with V_{S30} and the map for a firm-rock site condition. Areas with somewhat lower ground

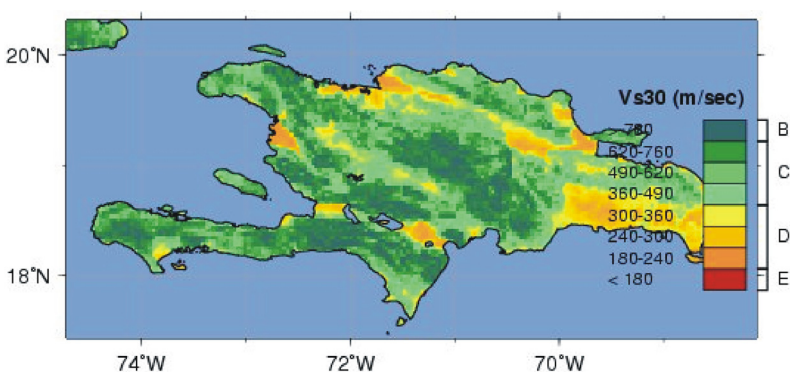

Figure 7. Map of V_{S30} derived from the topographic slope (from D. Wald, written comm.).

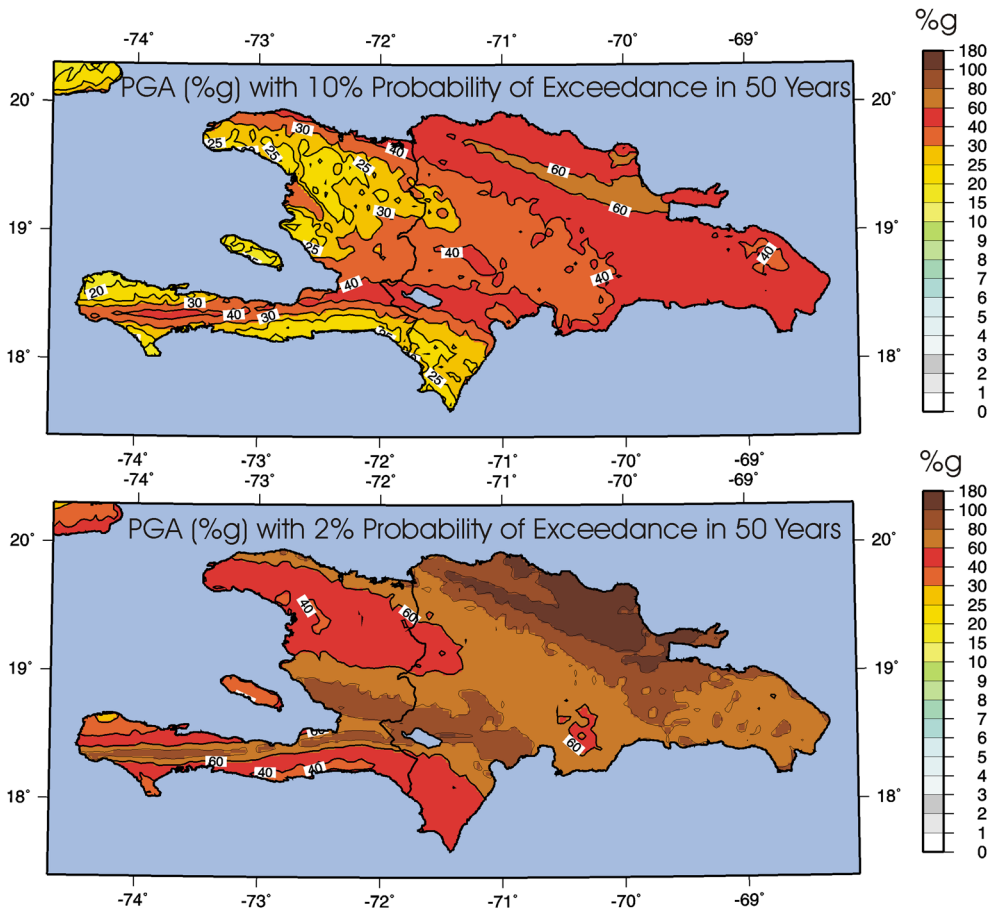

Figure 8. Hazard maps using grid of V_{S30} values shown in Figure 7: (top) PGA (%g) with 10% probability of exceedance, (bottom) PGA (%g) with 2% probability of exceedance in 50 years.

motions away from the active faults exhibit an increase in PGA of about 20%. Amplification at soil sites would be larger for the 0.5 and 1 Hz spectral accelerations.

We note that these maps do not include topographic amplification from ridges. Hough et al. (2010) report substantial amplification of aftershock recordings along a ridge on the hillside south of Port-au-Prince. They proposed that this amplification explained the large amount of damage along the ridge from the main shock. Thus, hazard maps with site amplification based on V_{S30} could underestimate shaking in areas with topographic amplification.

CONCLUSIONS AND RECOMMENDATIONS FOR FUTURE WORK

The hazard maps for Haiti quantify the high seismic hazard throughout the country and especially along the Enriquillo-Plantain Garden and Septentrional Faults. The high hazard along the Matheux-Neiba fault at 2% PE in 50 years is less certain, given that the slip rate used

is a maximum estimate from the GPS data. This fault deserves more study to better resolve its slip rate, identify its paleoearthquake chronology, and improve our assessment of its hazard.

Much more geologic and geophysical field work needs to be done to better constrain the slip rates of the major faults, chronicle the dates of prehistoric earthquakes, identify and characterize other crustal faults, and therefore improve the hazard maps. Direct mapping of site conditions, identification of topographic amplification, and determination of regionally specific attenuation relations are also important for improving the hazard maps.

The initial seismic hazard maps presented here should be considered for urban planning and building design applications as the reconstruction of Haiti progresses. These maps could be used together with maps of local soil conditions (e.g., Cox et al. 2011) for building codes to guide earthquake-resistant construction in Haiti.

ACKNOWLEDGMENTS

We thank Mark Petersen, David Perkins, Paul Mann, and two anonymous reviewers for their helpful reviews of the paper. We appreciate discussions on seismic hazard of Hispaniola with William McCann, Roland LaForge, William Bakun, Uri ten Brink, Carol Prentice, and Craig Weaver. David Wald produced the map of V_{S30} in Figure 7.

REFERENCES

Ali, S. T., Freed, A. M., Calais, E., Manaker, D. M., and McCann, W. R., 2008. Coulomb stress evolution in northeastern Caribbean over the past 250 years due to coseismic, postseismic, and interseismic deformation, *Geophysical Journal International* **174**, 904–918.

Atkinson, G. M., and Boore, D. M., 2003. Empirical ground-motion relations for subduction-zone earthquakes and their application to Cascadia and other regions, *Bulletin of the Seismological Society of America* **93**, 1703–1729.

Boore, D. M., and Atkinson, G. M., 2008. Ground-motion prediction equations for the average horizontal component of PGA, PGV, and 5%-damped PSA at spectral periods between 0.01 s and 10.0 s, *Earthquake Spectra* **24**, 99–138.

Byrne, D. E., Suarez, G., and McCann, W. R., 1985. Muertos Trough subduction—microplate tectonics in the northern Caribbean, *Nature* **317**, 420–42.

Calais, E., Mazabraud, Y., Mercier de Lepinay, B., Mann, P., Mattioli, G., and Jansma, P., 2002. Strain partitioning and fault slip rates in the northeastern Caribbean from GPS measurements, *Geophysical Research Letters* **29**, 1856–1860.

Calais, E., Freed, A., Mattioli, G., Amelung, F., Jonsson, S., Jansma, P., Hong, S. H., Dixon, T., Prépetit, C., and Momplaisir, R., 2010. Transpressional rupture of an unmapped fault during the 2010 Haiti earthquake, *Nature Geoscience* **3**, 794–799.

Campbell, K. W., and Y. Bozorgnia, 2008. NGA ground motion model for the geometric mean horizontal component of PGA, PGV, PGD and 5% damped linear elastic response spectra for periods ranging from 0.01 to 10 s, *Earthquake Spectra* **24**, 139–172.

Chiou, B. S. J., and Youngs, R. R., 2008. Chiou-Youngs NGA ground motion relations for the geometric mean horizontal component of peak and spectral ground motion parameters, *Earthquake Spectra* **24**, 173–216.

Cornell, C. A., 1968. Engineering seismic risk analysis, *Bull. Seism. Soc. Am.* **58**, 1583–1606.

Cox, B., Bachhuber, J., Rathje, E., Wood, C., Dulberg, R., Kottke, A., Green, R., and Olson, S., 2011. Shear wave velocity- and geology-based seismic microzonation of Port-au-Prince, Haiti, submitted for publication in *Earthquake Spectra*, this issue.

DeMets, C., Jansma, P. E., Mattioli, G. S., Dixon, T. H., Farina, F., Bilham, R., Calais, E., and Mann, P., 2000. GPS geodetic constraints on Caribbean-North America plate motion, *Geophysical Research Letters* **27**, 437–441.

Dolan, J. F., and Wald, D. J., 1998. The 1943–1953 north-central Caribbean earthquakes: active tectonics setting, seismic hazards, and implications for Caribbean-North America plate motions, in *Active Strike-slip and Collisional Tectonics of the Northern Caribbean Plate Boundary Zone, Special Paper No. 326* (J. F. Dolan and P. Mann, eds.), Geological Society of America, Boulder, CO, 143–170.

Engdahl, E. R., and Villasenor, A., 2002. Global seismicity—1900–1999, in *International Handbook of Earthquake and Engineering Seismology* (W. H. K. Lee, H. Kanamori, P. C. Jennings, and C. Kisslinger, eds.), International Association of Seismology and Physics of the Earth's Interior (IASPEI), 665–690.

Frankel, A., Mueller, C., Barnhard, T., Perkins, D., Leyendecker, E., Dickman, N., Hanson, S., and Hopper, M., 1996. *National Seismic Hazard Maps: Documentation June 1996, USGS Open File Report 96-532*, U.S. Geological Survey, Reston, VA.

Frankel, A. D., 1995. Mapping seismic hazard in the central and eastern United States, *Seismological Research Letters* **66**, 8–21.

Frankel, A., Mueller, C., Barnhard, T., Leyendecker, E., Wesson, R., Harmsen, S., Klein, F., Perkins, D., Dickman, N., Hanson, S., and Hopper, M., 2000. USGS national seismic hazard maps, *Earthquake Spectra* **16**, 1–19.

Frankel, A., Harmsen, S., Mueller, C., Calais, E., and Haase, J., 2010. *Initial Seismic Hazard Maps for Haiti, USGS Open File Report 2010-1067*, U.S. Geological Survey, Reston, VA.

Hayes, G. P., Briggs, R. W., Sladen, A., Fielding, E. J., Prentice, C., Hudnut, K., Mann, P., Taylor, F. W., Crone, A. J., Gold, R., Ito, T., and Simons, M., 2010. Complex rupture during the 12 January 2010 Haiti earthquake, *Nature Geoscience* **3**, 800–805.

Hough, S. E., Altidor, J. R., Anglade, D., Given, D., Janvier, M. G., Maharray, J. Z., Meremonte, M., Saint-Louis Mildor, B., Prepetit, C., and Yong, A., 2010. Localized damage caused by topographic amplification during the 2010 M7.0 Haiti earthquake, *Nature Geoscience* **3**, 778–782.

Kelleher, J., Sykes, L., and Oliver, J., 1973. Possible criteria for predicting earthquake locations and their application for major plate boundaries of the Pacific and the Caribbean, *Journal of Geophysical Research* **78**, 2547–2585.

Ladd, J. W., Worzel, J. L., and Watkins, J. S., 1977. Multifold seismic reflection records from the northern Venezuela Basin and the north slope of the Muertos Trough, in *Island Arcs, Deep Sea Trenches, and Back Arc Basins* (N. I. Talwani and W. C. Pitman, III, eds.), American Geophysical Union, Washington, DC, 41–56.

Manaker, D. M., Calais, E., Freed, A. M., Ali, S. T., Przybylski, P., Mattioli, G., Jansma, P., Prepetit, C., and de Cahbalier, J. B., 2008. Interseismic plate coupling and strain partitioning in the northeastern Caribbean, *Geophysical Journal International* **174**, 889–903.

Mann, P., Burke, K., and Matumoto, T., 1984. Neotectonics of Hispaniola: plate motion, sedimentation, and seismicity at a retraining bend, *Earth Planetary Science Letters* **70**, 311–324.

Mann, P., Taylor, F. W., Edwards, R. L., and Ku, T-L, 1995. Actively evolving microplate formation by oblique collision and sideways motion along strike-slip faults: An example from the northeastern Caribbean plate margin, *Tectonophysics* **246**, 1–69.

Mann, P., Prentice, C. S., Burr, G., Pena, L. R., and Taylor, F. W., 1998. Tectonic geomorphology and paleoseismology of the Septentrional fault system, Dominican Republic, in *Active Strike-slip and Collisional Tectonics of the Northern Caribbean Plate Boundary Zone, Special Paper No. 326* (J. F. Dolan, and P. Mann, eds.), Geological Society of America, Boulder, CO, 63–123.

Mann, P., Calais, E., Ruegg, J.-C., DeMets, C., Dixon, T. H., Jansma, P. E., and Mattioli, G. S., 2002. Oblique collision in the northeastern Caribbean from GPS measurements and geological observations, *Tectonics* **21**, 1057–1083.

McCann, W. R., 2006. Estimating the threat of tsunamagenic earthquakes and earthquake induced landslide tsunamis in the Caribbean, in *Caribbean Tsunami Hazard* (M. Aurelio and L. Philip, eds.), World Scientific Publishing, Singapore, 43–65.

Momplaisir, R., 1986. *Contribution à l'Étude Géologique de la Partie Orientale du Massif de la Hotte (Presqu'Ile du Sud d'Haïti), Synthèse Structurale des Marges de la Presqu'Ile du Sud à Partir de Données Sismiques*, Ph.D. thesis, University of Paris VI.

Mueller, C., Hopper, M., and Frankel, A., 1997. *Preparation of Earthquake Catalogs for the National Seismic Hazard Maps, USGS Open File Report 97-464*, U.S. Geological Survey Reston, VA.

Mueller, C., Frankel, A., Petersen, M., and Leyendecker, E., 2010. New seismic hazard maps for Puerto Rico and the U.S. Virgin Islands, *Earthquake Spectra* **26**, 169–186.

Petersen, M., Frankel, A., Harmsen, S., Mueller, C., Haller, K., Wheeler, R., Wesson, R., Zeng, Y., Boyd, O., Perkins, D., Luco, N., Field, E., Wills, C., and Rukstales, K., 2008. *Documentation for the 2008 Update of the United States National Seismic Hazard Maps: USGS Open File Report 2008–1128*, U.S. Geological Survey, Reston, VA.

Prentice, C. S., Mann, P., Pena, L. R., and Burr, G., 2003. Slip rate and earthquake occurrence along the central Septentrional fault, North American-Caribbean plate boundary, Dominican Republic, *Journal of Geophysical Research* **108**, 2149–2166.

Prentice, C. S., Mann, P., Crone, A. J., Gold, R. D., Hudnut, K. W., Briggs, R. W., Koehler, R. D., and Jean, P., 2010. Seismic hazard of the Enriquillo-Plantain Garden fault in Haiti inferred from palaeoseismology, *Nature Geosciences* **3**, 789–793.

Pubellier, M., Mauffret, A., Leroy, S., Vila, J. M., and Helliot, A., 2000. Plate boundary readjustment in oblique convergence: example of the Neogene of Hispaniola, Greater Antilles, *Tectonic* **19**, 630–648.

Shedlock, K. M., 1999. Seismic hazard map of North and Central America and the Caribbean, *Annali di Geofisica* **42**, 977–997.

Scherer, J., 1912. Great earthquakes in the island of Haiti, *Bull. Seism. Soc. of Am.* **2**, 161–180.

Tanner, J. G., and Shepherd, J. B., 1997. *Seismic Hazard in Latin America and the Caribbean, Project Catalog and Seismic Hazard Maps*, *Vol. 1*, International Development Research Centre, Ottawa, Canada, 143 pp.

ten Brink, U. S., Marshak, S., and Granja Bruna, J-L, 2009. Bivergent thrust wedges surrounding island arcs: insights from observations and sandbox models of the northeastern Caribbean plate, *Geol. Soc. Am. Bull.* **121**, 1522–1536.

Wald, D. J., and Allen, T.I., 2007. Topographic slope as a proxy for seismic site conditions and amplification, *Bull. Seism. Soc. of Am.* **97**, 1379–1395.

Wells, D. L., and Coppersmith, K. J., 1994. New empirical relationships among magnitude, rupture length, rupture width, rupture area, and surface displacement, *Bull. Seism. Soc. of Am.* **84**, 974–1002.

Weichert, D. H., 1980. Estimation of the earthquake recurrence parameters for unequal observation periods for different magnitudes, *Bull. Seism. Soc. of Am.* **70**, 1337–1346.

Youngs, R. R., Chiou, S. -J., Silva, W. J., and Humphrey, J. R., 1997. Strong ground motion attenuation relationships for subduction zone earthquakes, *Seismological Research Letters* **68**, 58–73.

Zhao, J. X., Zhang, J., Asano, A., Ohno, Y., Oouchi, T., Takahashi, T., Ogawa, H., Irikura, K., Thio, H. K., Somerville, P. G., Fukushima, Y., and Fukushima, Y., 2006. Attenuation relations of strong ground motion in Japan using site classification based on predominant period, *Bull. Seism. Soc. of Am.* **96**, 898–913.

(Received 23 September 2010; accepted 16 March 2011)